Model Predictive Control and Service Life Monitoring for Molten Salt Solar Power Towers

Wolfgang Grote-Ramm[1] iD, Felix Schönig[2] iD, Peter Schwarzbözl[3] iD, Maximilian Drexelius[3] iD, Daniel Maldonado Quinto[3], and Matthias Binder[2] iD

[1] University of Applied Sciences Düsseldorf, Germany

[2] MAN Energy Solutions SE, Germany

[3] German Aerospace Center (DLR), Institute of Solar Research, Germany

*Correspondence: Wolfgang Grote-Ramm, wolfgang.grote@hs-duesseldorf.de

Abstract. A two-component system for control and monitoring of solar power towers with molten salt receivers is proposed. The control component consists of a model predictive control application (MPC) with a flexible objective function and on-line tunable weights, which runs on a Industrial PC and uses a reduced order dynamic model of the receiver's thermal and flow dynamics. The second component consists of a service-life monitoring unit, which estimates the service-life consumption of the absorber tubes depending on the current mode of operation based on thermal stresses and creep fatigue in the high temperature regime. The calculation of stresses is done based on a detailed finite element study, in which a digital twin of the receiver was developed. By parallelising the model solver, the estimation of service-life consumption became capable of real-time operation. The system has been implemented at a test facility in Jülich, Germany, and awaits field experiments. In this paper, the modeling and architecture are presented along simulation results, which were validated on a hardware-in-the-loop test bench. The MPC showed good disturbance rejection while respecting process variable constraints during the simulation studies.

Keywords: Solar Power Tower, Molten Salt, Model Predictive Control, Dynamic Modeling, Digital Twin, Service-Life Monitoring, Predictive Maintenance

1. Introduction

Solar power towers with molten salt as heat transfer fluid (HTF) achieve high efficiencies and enable convenient integration of energy storage into the plant. Commercially used molten salts and receiver materials are prone to excessive salt decomposition, material corrosion and thermal stresses when exposed to temperatures above a critical limit for a certain amount of time. Therefore, operation and control strategies for solar power towers must meet complex requirements: Firstly, the effects of disturbances (fluctuations) of solar irradiance and other environmental factors on the HTF temperature must be rejected quickly and the plant be kept within its allowed operating range. Secondly, it is of economic interest to operate the plant close to the upper critical temperature limit since this maximises the power plant efficiency. Lastly, due to the natural fluctuation as well as the day-night cycle, the receiver components are exposed to extreme cyclical thermal stresses. To ensure reliable long-term operation, they must be inspected regularly and exchanged, if necessary. The uncertainty of maintenance and replacements, however, impedes the goal of maximising efficiency and profitability through stable,

long-time plant operation. This paper presents an advanced control and monitoring system to overcome these challenges.

The cyclical load due to thermal stresses in the receiver materials was modelled and implemented into a monitoring unit, which is presented in Sec. 1. With this, the impact of a mode of operation on the service life of the receiver components is predicted and can be considered in the control strategy. Furthermore, an MPC algorithm was implemented to operate the process close to its admissible limits, to react quickly on measured and predicted fluctuations of irradiation, and to limit temperature gradients within the receiver material. This control unit is discussed in Sec. 2 along with simulation results.

1.1 System description

A CAD model of the test receiver at the test facility in Jülich, Germany is depicted in Fig. 1 (left) while the flow path of the HTF is sketched right. There are eight panels, each containing two absorber tubes, through which the HTF flows in parallel. At the interconnection between two panels are separated header elements, which mix and redirect the flow from the twotubes. The absorber tubes are irradiated on one side only, the back side faces an isolating wall. A control valve is positioned upstream of the receiver, while the outlet feeds, passing through a short piping system, an outlet tank.
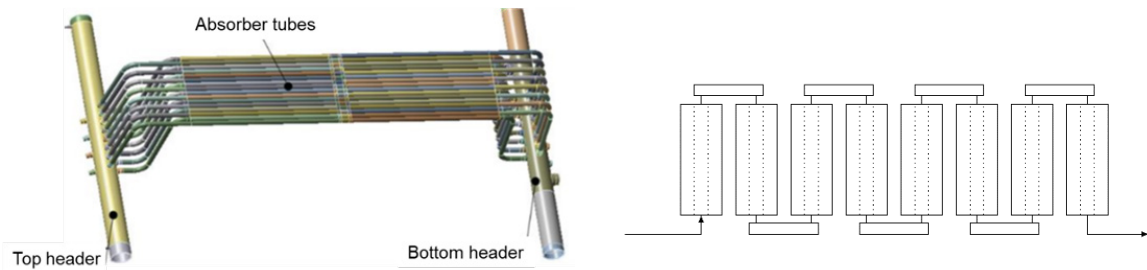

Figure 1. *Left: Exemplary representation of the 3D geometry of the absorber tubes, top and bottom header of the test receiver (cf. [1]), right: sketch of HTF flow path.*

Fig. 2 gives an overview of the control and monitoring systems. The Receiver-PCS (Process Control System) communicates live measurements from the plant to the control and service life monitoring units.

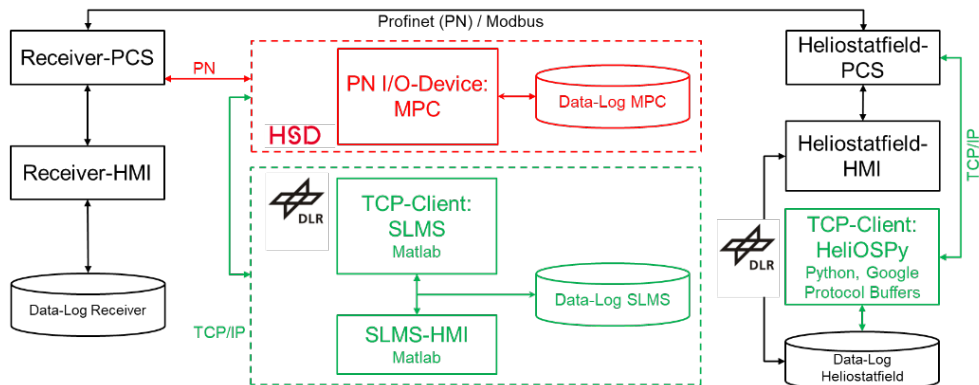**Figure 2.** *Definition of the software interfaces and the integration within the receiver and heliostat software environment.*

During receiver operation, the service life monitoring system (SLMS) receives the present flux density and receiver inlet conditions from the receiver PCS. With this data, the local load conditions are determined, and the service life consumption is derived as described in

Sec. 2. The accumulated service life consumption from creep and fatigue can result in a recommendation for a service life optimized control strategy. It is up to the operator to decide how this recommendation is considered in the MPC objective function. Furthermore, live tuning of the MPC algorithm is also done via the PCS.

2. Service life monitoring system

Cyclic loads and thermal gradients during transient receiver operation challenge the operation of molten salt central receivers. Therefore, the quality of a control strategy should be assessed not only in terms of the overall efficiency, but also in terms of its service life consumption. Correctly estimated stresses in the metal absorber tubes and headers form the basis for monitoring the service life consumption.

2.1 Thermomechanical components and receiver model

The first step is the development of a 1D-model for the molten salt test receiver. The individual components are modelled using the finite element method, considering radiation exchange with the environment and the neighbouring tubes, convection and a model for the mechanical boundary conditions. These 1D-component models are validated by a comparison with the equivalent stress $\sigma_{eq,max}$ obtained from a detailed 3D-CFD model. The comparison between the 1D- and 3D-model is undertaken for five representative stationary load cases with varying inlet bulk velocities, inlet temperatures and flux densities. The absorber tube and header models are connected sequentially and in parallel to assemble a digital twin of the entire receiver. With the validated 1D-model, load conditions and resulting local equivalent elastic stresses $\sigma_{eq}^{el}(x,t)$ and strains $\varepsilon_{eq}^{el}(x,t)$ are calculated for a predefined state space that covers the relevant range of expected flux densities, HTF inlet temperatures and mass flows.

2.2 Service life estimation procedure

In a second step, the service life consumption is estimated based on the determined stress conditions. In this determination, thermo-cyclic loads as well as creep-fatigue in the high temperature regime are considered. During the operation of the receiver, the equivalent elastic stresses $\sigma_{eq}^{el}(x,t)$ are determined via a multiple linear regression from the pre-calculated state space for each time step based on the measured quantities.

Furthermore, the rainflow analysis approach [2] is applied on the calculated strain time series $(\sigma_{eq}^{el}(x,t))$ in order to derive the number of load cycles, acting upper and lower stresses, holding times and reference temperatures within each cycle l. For each load cycle the elastic values are further modified in order to consider plastic effects depending on the operational regime in accordance with e.g. [3], which gives the equivalent stresses $\sigma_{eq}(x,\Delta t_i)$ and strains $\Delta \varepsilon_{eq}(x,\Delta t_i)$.

Based on those results, for each load cycle the local creep and fatigue damage $D_c(x,t_i)$, $D_f(x,t_i)$ are determined from the linear damage rule in accordance with the procedure by [4]. The times to rupture at upper (o) and lower (u) stress level $t_{c,o}$ and $t_{c,u}$ are determined from stress-to-rupture curves depending on the reference temperature during the load cycle and the equivalent stress. The local creep damage D_c is then derived from the linear damage rule as in

$$D_c = SF_c(x)(\frac{\Delta t_{H,o,eff}^l}{t_{c,o}} + \frac{\Delta t_{H,u,eff}^l}{t_{c,u}}) \tag{1}$$

with the dwell times at each cycle at upper (o) and lower (u) stress level $\Delta t_{H,o,eff}^l$ and $\Delta t_{H,u,eff}^l$ and the local safety factors $SF_c(x)$.

Regarding the fatigue damage D_f, the number of allowable cycles to fatigue $N_f(x, \Delta t_i)$ are determined from design fatigue curves (cf. [5]) and the fatigue damage is derived from the linear damage rule as in

$$D_f = SF_f(x) \frac{N_l}{N_f} \tag{2}$$

with N_l cycles within each load cycle and the safety factors $SF_f(x)$.

The local absolute damage from creep and fatigue during each load cycle is finally derived from an interaction model and linearly accumulated over each cycle in order to determine the combined creep-fatigue damage, which is compared to the damage limit D_L of the material to estimate the service life consumption.

3. Model predictive control unit

The MPC was designed to control the receiver outlet temperature and respect process constraints. In the following sections, the dynamic model – from which the MPC prediction model is derived – and the MPC algorithm are presented.

3.1 Dynamic model of the central tower receiver

Employing a model predictive control unit requires a dynamic model that can predict the states of the desired control variables. While accuracy is a concern, increasing the model complexity beyond a certain point diminishes the suitability of the model for MPC, because the predictions become increasingly computationally expensive. Since the MPC unit runs on a designated hardware in the actual plant in real-time, computational resources are limited. Hence the model must make a trade-off between model accuracy and simplicity (or low computational effort). The dynamic model consists of two parts: Firstly, a thermal model of the absorber tube temperatures and fluid temperatures, and secondly, a simplified dynamic model of the volumetric flow that is manipulated with a control valve.
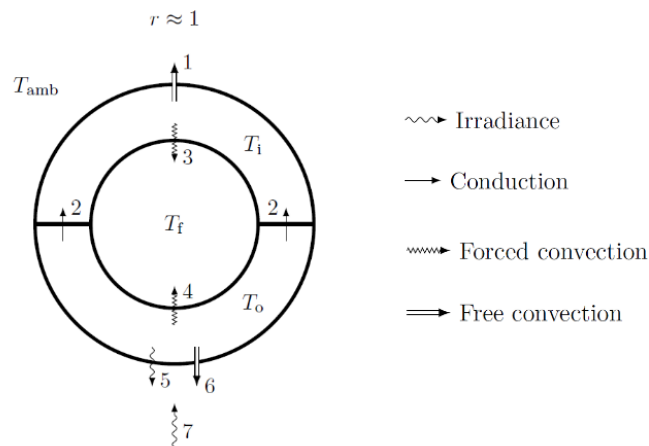

Figure 3. Cross-sectional view of the two-shell discretisation showing the considered heat transfers.

With the goal of keeping the model complexity low, the symmetry of the parallel flow paths is exploited and, thus, only one absorber tube is modelled per panel. Because of the one-sided irradiation, the absorber tube is divided into an outer and inner shell (see Fig. 3). With this modelling approach and such a coarse discretization, the predicted temperature is a caloric mean temperature for the element. It is obvious, that peak temperatures will be much

higher. However, they are only supposed to approximate dynamics of the thermal behaviour to the MPC. The energy balance for the outer shell reads

$$m_{shell}c_{shell}\,\dot{T}_o = \dot{Q}_7 - \dot{Q}_2 - \dot{Q}_4 - \dot{Q}_5 - \dot{Q}_6 \tag{3}$$

and for the inner shell it is

$$m_{shell}c_{shell}\,\dot{T}_i = \dot{Q}_2 - \dot{Q}_1 - \dot{Q}_3. \tag{4}$$

Finally, the energy balance for the fluid element inside the absorber tube must be

$$m_{fluid}\,c_f\,\dot{T}_f = \frac{\alpha_{i,f}A_i}{2}\left(T_i - T_f\right) + \frac{\alpha_{o,f}A_i}{2}\left(T_o - T_f\right) - \dot{m}\,c_{fluid}\left(T_f - T_{f,in}\right). \tag{5}$$

The respective heat flow rates are

$$\dot{Q}_1 = \frac{\alpha_{i,amb}A_o}{2}\left(T_i - T_{amb}\right) \tag{6}$$

$$\dot{Q}_2 = \lambda\,A_{con}\frac{T_o - T_i}{\Delta r} \tag{7}$$

$$\dot{Q}_3 = \frac{\alpha_{i,f}A_i}{2}\left(T_i - T_f\right) \tag{8}$$

$$\dot{Q}_4 = \frac{\alpha_{o,f}A_i}{2}\left(T_o - T_f\right) \tag{9}$$

$$\dot{Q}_5 = \frac{A_o}{2}\frac{\gamma}{2\pi}\,\sigma\,\varepsilon\,(T_o^4 - T_{amb}^4) \tag{10}$$

$$\dot{Q}_6 = \frac{\alpha_{o,amb}A_o}{2}\left(T_o - T_{amb}\right) \tag{11}$$

$$\dot{Q}_7 = q\,A_{proj} \tag{12}$$

with the inner tube shell area A_i, the outer tube shell area A_o, the contact area between the inner and outer shell halves A_{con}, the projection area $A_{proj} = d_o\,\Delta x$ and the angle γ for incoming irradiation that excludes radiation exchange with neighbouring absorber tubes. The heat transfer coefficients $\alpha_{i,f}$, $\alpha_{o,f}$ are calculated for turbulent flow in tubes, while free convection effects are covered by the coefficients $\alpha_{i,amb}$ and $\alpha_{o,amb}$.

To model the inertia of the HTF mass in the system and incorporate the pressure losses, the hydraulic model of the receiver consists of a resistance element R and an inertia element I, which are connected in series (see Fig. 4).
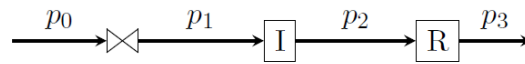

Figure 4. *Simplified hydraulic model: The inlet tank pressure p_0 is upstream of the control valve. The receiver induces a transient (I) pressure loss as well as a pressure loss due to flow resistance (R).*

The pressure loss across each element is considered. By summing up the individual pressure losses (across the valve, due to unsteady changes in the volumetric flow rate and due to resistance/viscosity effects) to retain the total pressure loss $p_0 - p_3$, a differential equation describing the transient flow dynamics results:

$$\frac{\partial \dot{V}}{\partial t}\frac{\rho_f L}{A} = p_0 - p_3 - \left(\frac{\dot{V}}{K_v}\right)^2\frac{1\text{bar}\,\rho_f}{10^3\frac{\text{kg}}{\text{m}^3}} - \dot{V}^2 R. \tag{13}$$

3.2 Model predictive control algorithm

The predictive control algorithm is based upon linearised and time-discretised state space prediction models of the aforementioned dynamic model and its formulation is generally adopted from [6], [7]. The controller minimises a cost function consisting of two terms representing control errors and actuator movement:

$$\underset{u(k),\ k=1\ldots Hu}{\arg\min}\quad J = \sum_{k=1}^{Hp} Q \cdot [T_{out,\text{setp}}(k) - T_{out,\text{pred}}(k)]^2 + \sum_{k=1}^{Hu} R \cdot [\Delta u(k)]^2 \qquad (14)$$

The squared control error of the predicted receiver HTF outlet temperature $T_{out,\text{pred}}$ with respect to the set point $T_{out,\text{setp}}$ is summed up over the prediction horizon Hp and weighted by a tuning factor Q. To be able to slow down the control action, the cost J also increases with the future squared actuator movement $\Delta u(k) = u(k) - u(k-1)$, weighted by R summed over the control horizon Hu. The quadratic cost function is subject to constraints. Firstly, the prediction model must be satisfied:

$$x(k) = A \cdot x(k-1) + B \cdot u(k) + E \cdot d(k), \qquad y(k) = T_{out,\text{pred}}(k) = C \cdot x(k) + z(k)\ \forall k. \qquad (15)$$

The model matrices A, B, C and E are obtained from the linearised Simulink model of the system. Since the linearised model is of high order ≈ 100, we applied order reduction to 25 states using balanced truncation. The state vector x is estimated by a time-discrete linear Kalman filter, d is the vector of the measured disturbances and comprises of measured flux density, receiver HTF inlet temperature, upstream and downstream pressures of the receiver and the ambient temperature.

While updated after each sample time $T_{cycle} = 250$ ms, vector d is considered to remain constant over Hp during every simulation run of the MPC. Unmeasured disturbances z are considered to prevent steady state errors, these are also estimated by the Kalman filter. Due to strongly nonlinear behavior of the underlying dynamic model that is mainly caused by varying system time constants at different mass flow rates, we use five different linearised models representing different operating points. The MPC algorithm selects the respective prediction model based on the measured HTF flow rate, where the selection mechanism is implemented with hysteresis to avoid spurious switching.

The following constraints regarding the manipulated and controlled variables are implemented:

$$u_{\min} < u(k) < u_{\max}, \qquad \dot{u}_{\min} < \frac{\Delta u(k)}{T_{\text{cycle}}} < \dot{u}_{\max}, \qquad T_{out,\text{pred}}(k) < T_{out,\max}\ \forall\, k, \qquad (16)$$

where the first and second constraint limit the valve opening in its feasible positions and velocities and the third constraint limits the HTF temperature to a maximum admissible value to avoid HTF decomposition. The MPC algorithm is programmed in C++, the optimisation problem arising from the MPC formulation is solved by the open source QP solver qpOASES [8]. The MPC is implemented on an industrial computer (Siemens IPC 627 E) running with a real-time Linux OS (Debian w/ Preempt-RT patch) interfacing with the plant distributed control system (DCS) via Profinet (see Fig. 2).

3.3 MPC Simulation Scenarios

To evaluate the proposed MPC concept we carried out simulation studies using the developed control algorithm on the IPC target platform. Since the real-world molten salt receiver has not yet been ready for testing, we used hardware-in-the-loop simulations using a dSPACE system to execute the original nonlinear simulation model instead. MPC behavior is compared to a classic PI-controller which was tuned to a moderate fast behavior with an appropriate integral time constant $T_i = 2.5 \cdot 2\,\pi/\omega_{gm} = 5$sec, with ω_{gm} denoting the phase-crossover frequency, and a controller gain of $K_c = 1.1$ to achieve a phase margin of $70°$ providing sufficient robustness. The MPC was set to a sampling time of $T_{cycle} = 250$ ms, a prediction horizon of $Hp = 200$, a control horizon of $Hu = 10$, leading to a simulation of the immediate 50 seconds. In the

scenario (Fig. 5), a set point step down and step up were simulated ($\Delta T_{out,\text{setp}} = \mp 10\,\text{K}, t = 50\,sec, t = 100\,sec$), followed by a harsh "passing-cloud" event where the flux density changes step-wise by $\Delta S = \mp 200\,kW/m^2$ ($t = 150\,sec, t = 200\,sec$). At $t = 250\,sec$ and $t = 300\,sec$ we simulated a disturbance at the receiver inlet temperature of $\Delta T_{in} = \mp 10$ K. While the MPC handles step point changes faster, also the disturbance rejection of the MPC is faster and with less over- or undershooting compared to the PI controller.

The MPC's ability to cope with hardly predictable changes in flux density is the most important performance gain over the PI controlled system. This is crucial for both, the service life of the receiver and the stability of the HTF as such events produce strong overshoots in receiver material (differential) temperatures (Fig. 6) and HTF temperatures (Fig. 5), which can be mitigated substantially by quick controller response. The key factor here is to measure the flux density and to use it as disturbance input to the prediction model. It should be noted that the PI-controller performance could be increased as well to some extent by using additional disturbance feed-forward control. Another important feature of the MPC solution is its ability to account for constraints of the controlled variables, i.e. receiver outlet temperature, even on occurrence of disturbances. If that constraint (16.3) is activated, the controller will prevent violating the temperature limit as long as the latitude of the manipulated variables allow for that and thus supports mitigating HTF decomposition.
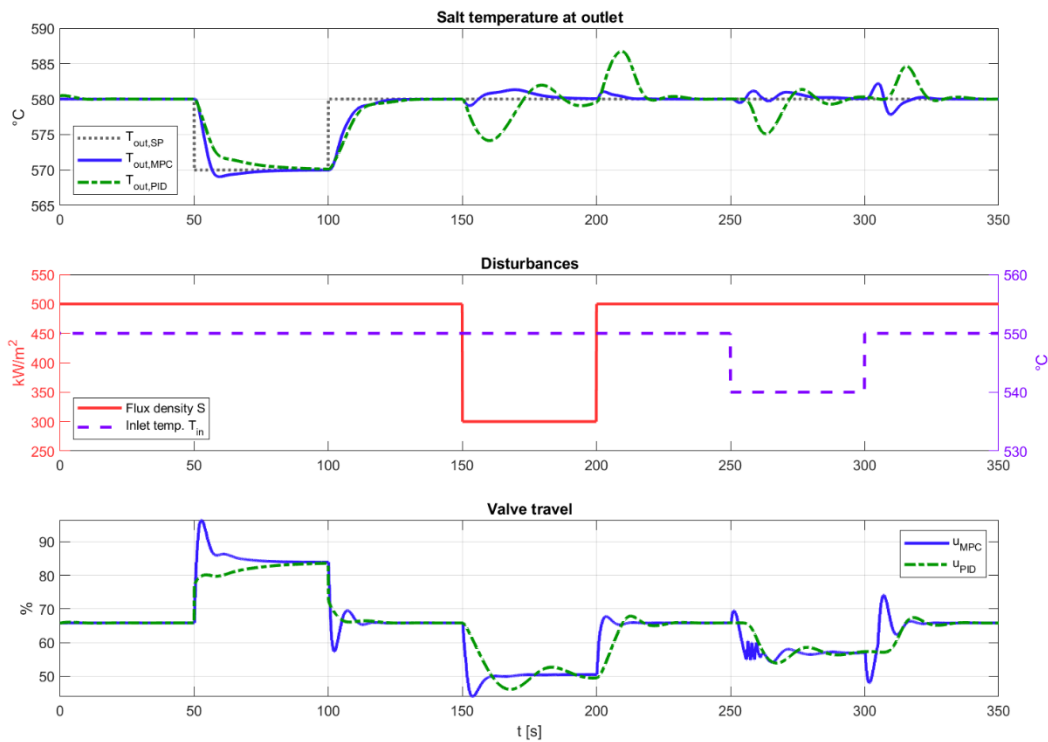

Figure 5. *Outlet temperature control scenario with MPC and PID controllers compared. Top: Outlet temperatures and set point, middle: disturbances flux density and inlet temperature, bottom: valve travel (controller outputs. The MPC was tuned to **Q**=6 and **R**=5.*
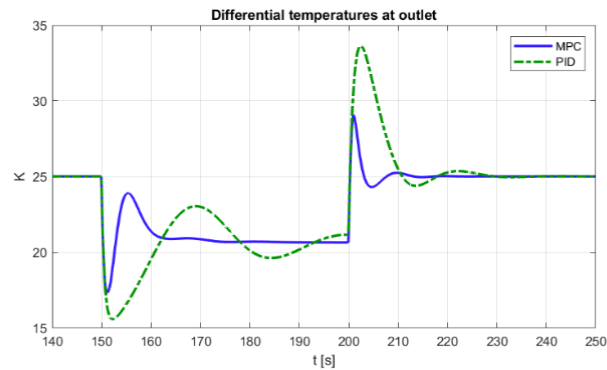
Figure 6. Receiver material differential temperatures during the "passing-cloud" scenario.

4. Conclusion and Outlook

In this paper we proposed a combined monitoring and control system for a solar tower receiver which aims to minimize the service life consumption during volatile operation resulting mainly from fluctuating irradiation. While the long-term operation is monitored and evaluated by the SLMS, the MPC covers fast fluctuations and avoids HTF and receiver material temperature peaks. Furthermore, the SLMS will be able to modify the MPC's cost function to find the best compromise between minimum service life consumption and exploiting admissible temperature limits to increase plant efficiency. Simulations in HiL-experiments show promising results; however, these shall be validated by measurement campaigns in the real plant in the near future.

Data availability statement

Not applicable.

Author contributions

The authors contributed equally to the paper.

Competing interests

The authors declare no competing interests.

Funding

References

[1] M. Binder et al. "Creep-fatigue evaluation according ASME III/5, Ed. 2019", Internal project report, November, 2020

[2] Standard practices for cycle counting in fatigue analysis. ASTM E 1049-85. ASTM International. 2005

[3] J. Bree, "Elastic-plastic behaviour of thin tubes subjected to internal pressure and intermittent high-heat fluxes with application to fast-nuclear-reactor fuel elements", Journal of

Strain Analysis, vol.2, no.3, pp. 226-238. July, 1967, doi: https://doi.org/10.1243/03093247V023226

[4] P.A. González-Gómez et al., "Calculating molten-salt central-receiver lifetime under creep-fatigue damage", Solar Energy, vol.213, no.1, pp. 180-197. January, 2021, doi: https://doi.org/10.1016/j.solener.2020.11.033

[5] M. Spiegel, "Life cycle assessment of DMV310Nsolar for the HPMSII solar test receiver", Conference: FVWHT Langzeitverhalten warmfester Stähle und Hochtempera-turwerkstoffe, December, 2020.

[6] J.M. Maciejowski, "Predictive Control with Constraints", 1st ed., Prentice Hall, England, 2002

[7] D. Mier, F. Möllenbruck, M. Jost, W. Grote, M. Mönnigmann, "Model predictive control of the steam cycle in a solar power plant", 9th IFAC International Symposium on Advanced Control of Chemical Processes, Whistler, 2015. https://doi.org/10.1016/j.ifacol.2015.09.052

[8] H.J. Ferreau et al., "qpOASES: A parametric active-set algorithm for quadratic program-ming", Mathematical Programming Computation vol. 6, no. 4, pp. 327-363, 2014